One-Dimensional ZnO Nanostructure Arrays: Synthesis and Characterization

Soumitra Kar,[†] Bhola Nath Pal,[‡] Subhadra Chaudhuri,*[,†] and Dipankar Chakravorty[‡]

DST Unit on Nano Science & Department of Materials Science and DST Unit on Nano Science & MLS Professor's Unit, Indian Association for the Cultivation of Science, Kolkata 700 032, India

Received: November 18, 2005; In Final Form: January 13, 2006

One-dimensional ZnO nanostructure arrays such as nanowires, nanonails, and nanotrees, have been synthesized by oxygen assisted thermal evaporation of metallic zinc on a quartz substrate over a large area. Morphological evolution of ZnO nanostructures at different time scales and different positions of the substrates have been studied by electron microscopy. A self-catalyzed vapor−liquid−solid (VLS) process is believed to be responsible for the nucleation and subsequently a vapor−solid process is operative for further longitudinal growth. The photoluminescence spectrum showed a weak UV and a broad green emission peak at 3.25 and 2.49 eV, respectively. The latter was attributed to the presence of zinc interstitial defects. Electrical resistivity as a function of temperature showed activated mechanisms to be present. The electrical response of the ZnO nanonail arrays to different gases (CO, NO_2, and H_2S) indicated that there could be possible application as gas sensors for this material.

1. Introduction

Zinc oxide is an important semiconductor with a wide band gap energy (3.3 eV) and a large exciton binding energy (60 meV) at room temperature. The exciton binding energy of ZnO is much higher than the thermal energy at room temperature (26 meV) and is also much higher than other prospective materials such as ZnSe (22 meV), ZnS (40 meV), and GaN (25 meV), which make it one of the outstanding semiconductors for lasing. ZnO is a very promising alternative in flat panel displays[1,2] to tin doped indium oxide (ITO). ZnO is also important for its wide range of applications as sensors,[3,4] photocatalyst[5] light emitting diodes and laser diodes in the UV−vis range,[6−8] etc. ZnO 1-D nanoforms are found to be highly suitable for nanoscale applications such as room temperature laser,[9] field effect transistor[10] nanoresonator,[11] etc. One-dimensional nanostructures, specially aligned ZnO nanoforms, are especially important for their enhanced optical properties.[9−10,12] Since Huang et al.[9] reported aligned ZnO nanowires via the Au catalyzed vapor−liquid−solid (VLS) process, several methods[9−20] have been reported to synthesize aligned ZnO 1-D nanoforms. Among these, thermal evaporation condensation is the common approach, but such processes require catalysts such as gold (Au),[9−10,12,13] Sn,[14] Co,[15] NiO,[16] etc. These catalysts will unavoidably influence the purity of the ZnO nanoforms and they could have an effect on the physical properties of these products. The noncatalytic approach has also been utilized to fabricate ZnO but only disarrayed nanoforms have been reported so far.[17,18] For the fabrication of ZnO 1-D nanostructure arrays, special kinds of substrates were used such as (110) sapphire substrates,[9] a heavily doped silicon-terminated silicon carbide (SiC) epilayer on either 4H- or 6H-SiC substrates,[10] or GaN, AlN, and AlGaN substrates.[13] Recently, ZnO nanowire arrays have been fabricated on c-oriented ZnO thin films without using a catalyst.[19] A new morphology called nanonails was produced by Lao et al.[20] by thermal evaporation of ZnO, In_2O_3, and graphite powders onto a graphite substrate at temperatures higher than 950 °C. Despite the progress in the synthesis of ZnO nanowire arrays it is still a challenge to fabricate 1-D ZnO nanostructure arrays on simple substrates by a noncatalytic approach.

In this paper we demonstrate fabrication of perfectly aligned 1-D nanoforms of ZnO by oxygen assisted thermal evaporation of metallic Zn powder on quartz substrate at 500 °C. ZnO nanowire and nanonail arrays have been produced over a large area without using any catalyst or any special substrates. ZnO nanotrees and nanosheets have also been produced at different conditions of the fabrication process. Optical and electrical properties of the ZnO nanowire and nanonail arrays have been investigated. We have also investigated the applicability of these ZnO 1-D nanoform arrays as gas sensors.

2. Experimental Section

A conventional horizontal tube furnace was used for the synthesis of ZnO nanostructures. The experimental setup consisted of a one-end open quartz tube fitted with a rotary vacuum pump and a gas inlet through a vacuum coupling.[21] Cleaned quartz plates were used as substrates. Commercial Zn powder (1 g) was loaded into a quartz boat. The quartz substrate was then placed over the quartz boat with the vertical distance between the Zn powder and the substrate being kept at 3 mm. It was then placed near the closed end of the quartz tube. The deposition system was then evacuated to a pressure of 10^{-3} Torr and subsequently Ar gas was passed through the system with a flow rate of 100 cm^3/min. The quartz tube was then inserted into a preheated tube furnace at 500 °C. After 5 min of deposition 5% oxygen was introduced along with the Ar gas and this was maintained for the entire deposition period. After a few minutes of deposition the quartz tube was taken out of the furnace to allow rapid cooling to room temperature. The deposition time was varied from 15 to 45 min. White wool like product was found on both sides of the quartz substrate as well as its edge facing the Zn vapor.

* Address correspondence to this author: Phone: +91-033-2473-4971. Fax: +91-033-2473-2805. E-mail: mssc2@iacs.res.in.

[†] DST Unit on Nano Science & Department of Materials Science.

[‡] DST Unit on Nano Science & MLS Professor's Unit.

10.1021/jp056673r CCC: $33.50
Published on Web 02/14/2006

The products were characterized by X-ray diffractometer (XRD, Seifert 3000P) with Cu Kα radiation and the compositional analysis was done by energy dispersive analysis of X-ray (EDAX, Kevex, Delta Class I). Microstructures of the nanoforms were studied by scanning electron microscopy (SEM, Hitachi S-2300) and transmission electron microscopy (TEM, JEOL 2010). The high-resolution transmission electron microscopic (HRTEM) images and the typical selected area electron diffraction (SAED) patterns of the ZnO nanoforms were also recorded. Optical absorption spectra of the products dispersed in spectroscopic grade ethanol were recorded by a spectrophotometer (Hitachi U 3410). Photoluminescence (PL) measurements were carried out at room temperature with a luminescence spectrometer (Hitachi, F2500), using 300 nm as the excitation wavelength. For electrical measurements two silver paint electrodes (supplied by B. V. Colloiden, The Netherlands) were applied on the surface of the nanoforms with a separation of 2 mm. The dc electrical resistances of the samples were measured by a Kiethley 617 electrometer over the temperature range 27−317 °C.

Gas sensing properties of the samples were also studied. Gases used were CO, NO_2, and H_2S. For this investigation N_2 gas mixed with the desired amount of the gaseous species (CO, NO_2, and H_2S) was passed through a sealed chamber at temperatures in the range 100−300 °C. Sample resistance was measured by a Kiethley 617 electrometer as a function of time.

3. Results and Discussion

A white layer was found to be deposited on both sides as well as at the edge of the quartz substrate, which faced the Zn vapor. In subsequent discussion we will refer to the surface facing the Zn powder as the bottom surface, the opposite face as the top surface, and the edge as the edge. Two representative XRD spectra are shown in Figure 1a revealing the wurtzite phase of ZnO (JCPDS card no. 36-1451). The overwhelming (002) peaks indicate that the preferred orientation of the ZnO crystals is along the *c*-axis. The chemical purity of the samples as well as their stoichiometry was tested by EDAX studies. The EDAX spectra given in Figure 1b show the presence of Zn and O as the only elementary components. Compositional analysis of the spectrum reveals oxygen deficiency in the samples (Zn:O = 58:42 in atomic ratio).

The morphologies of the products deposited on the top side of the substrates after different deposition periods are shown in Figure 2. Figure 2a shows the top view of the products deposited after 15 min of time revealing the formation of ZnO nanowire arrays over a large area. Diameters of these nanowires are of the order of 100 nm. Figure 2b shows the magnified SEM image of the products obtained after 30 min of deposition revealing the hexagonal cross-section of the nanowire arrays. But it is observed that the density of the nanowires is not uniform throughout the top surface but much more dense toward the end facing the incoming Zn vapors. This is clearly evident from the SEM image of this region shown in Figure 2c. The diameters of the hexagonal top of the nanowires vary from 100 to 200 nm. Figure 2d shows the cross-sectional view of the nanowire arrays, which indicates that these nanowires should be better termed as nanonails because of their peculiar morphology. The cross-section of these nanoforms is not uniform throughout their length but they are cone shaped toward their top. The length of these nanonails is ∼2 μm. Diameters of the lower straight portion of these nanonails are ∼75 nm. For a deposition period of 45 min these cones become sharper as revealed from the SEM images shown in Figure 2e,f. Also the diameters of the

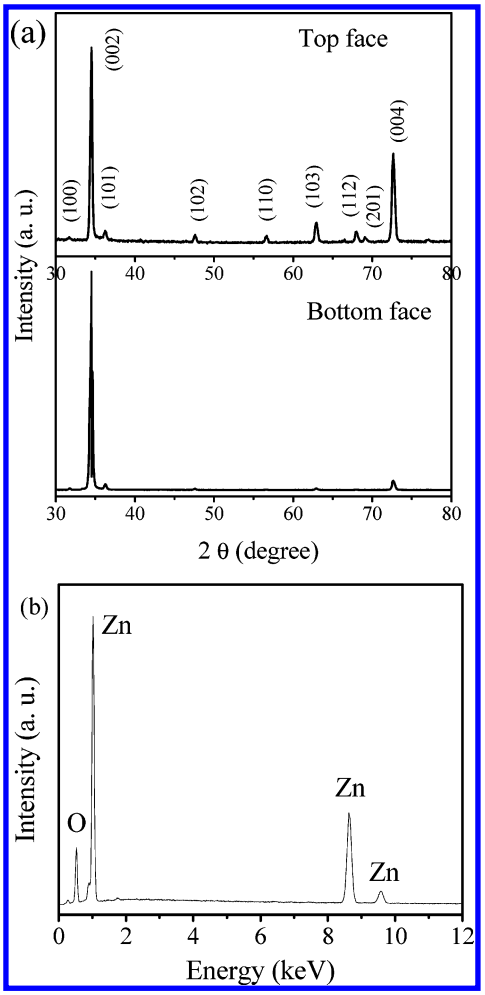

Figure 1. (a) XRD pattern of the ZnO nanoforms produced at the top and bottom surface of the quartz substrate and (b) EDAX spectrum of a representative ZnO nanowire sample.

stem of the nanonails decrease gradually toward their top. These results indicate that with a change in the deposition time the length as well as the shape of the ZnO nanoforms change. The nanowires, which are initially straight, gradually become nanonails and the cap region of the nanonails becomes shorter with time.

Figure 3 shows the SEM images of the products obtained at the bottom surface of the quartz substrates after different deposition times. Figure 3a shows the formation of ZnO nanowire arrays over a large area after only 15 min. After 25 min of deposition the length of these nanowires increased so much that bending appeared in the wires (Figure 3b). It is observed that if the deposition period is increased further to 30 min not only the length of these nanowires increased to destroy the alignment but also a foggy material appeared surrounding the nanowires as revealed by the SEM image shown in Figure 3c. After 45 min this foggy material becomes the ZnO nanosheet (Figure 3d). These images indicate that the length of the nanowires formed in the bottom surface increases much faster than those at the top surface.

The morphologies of the products obtained at the edge are distinct from what are obtained at the two surfaces of the quartz substrates. Figure 4a shows that ZnO nanonails are produced at the edge even after 15 min of deposition. Figure 4b shows the cross-sectional view of these nanonails. The diameters of the top of the nails are seen to vary from 200 to 400 nm—much larger than the ones obtained at the top surface. Also the cross-section of the stem of these nanonails is not uniform but

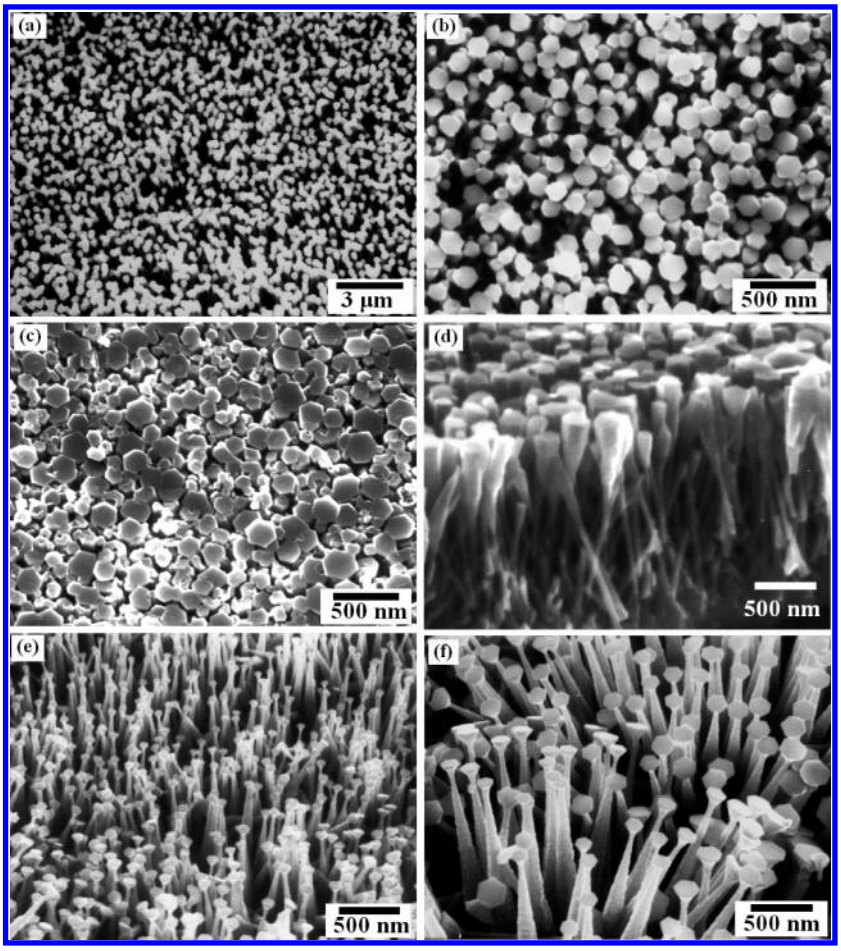

Figure 2. SEM images of the ZnO 1-D nanoforms after different deposition times at the central position of the top surface: (a) 15, (b) 30, and (e) 45 min. The images in parts c and d show the top and cross-sectional view of the nanoforms produced toward the edge facing the incoming vapor, after 30 min. The image in part f shows the samples obtained after 45 min at this edge area.

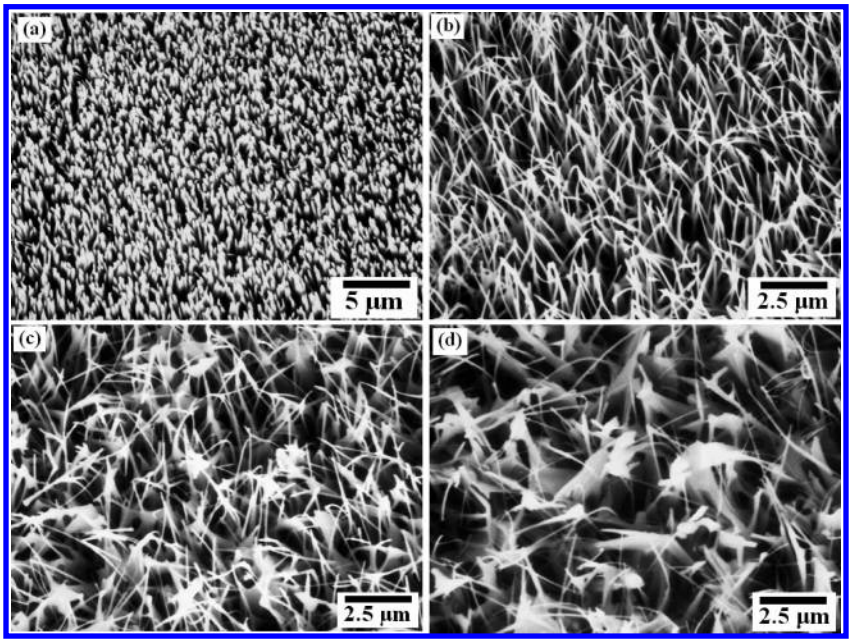

Figure 3. SEM images of the ZnO nanoforms produced at the bottom face after different deposition times: (a) 15, (b) 25, (c) 30, and (d) 45 min.

like those of the products deposited at the top after 45 min of deposition. It is interesting to observe that multiarmed ZnO nanonails (Figure 4c,d) were obtained after 30 min of deposition time. The magnified SEM image in Figure 4d shows the formation of new nanonails from the stem of one nanonail, like the formation of branches of trees. With time this type of branching continues to give the ZnO nanoforms the real look of trees with several branchings (Figure 4e,f). The diameters of the branches gradually decrease. Cone shaped structures are also visible at the top of each branch but with much smaller

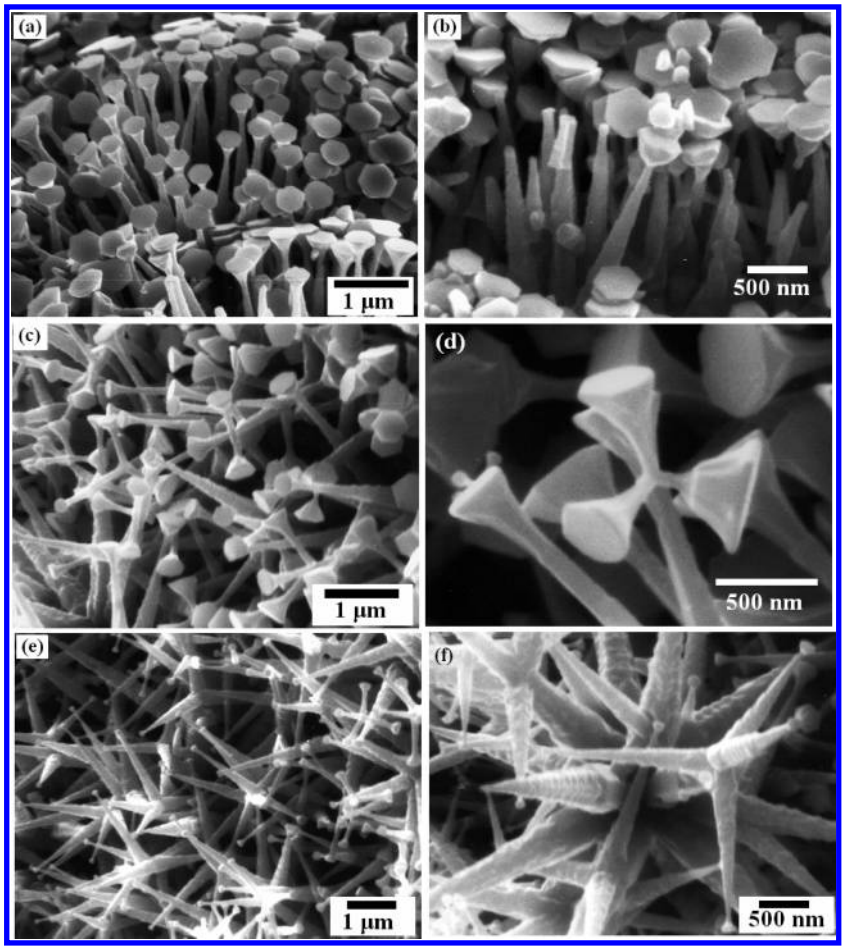

Figure 4. SEM images of the nanoforms deposited at the edge of the quartz substrate that faces the source vapor after different times: (a, b) 15, (c, d) 30, and (e, f) 45 min.

dimension. From the SEM images it can be seen that unlike the nanoforms produced at the top and bottom surfaces the surfaces of the nanoforms produced at the edge are quite rough.

The TEM image shown in Figure 5a reveals the morphology of a single ZnO nanonail produced at the top surface after 30 min of deposition. The ripple-like contrasts observed in the straight portion of the nanonail might be due to the strains developed in the nanoforms during formation. Figure 5b reveals the morphology of the ZnO nanowires produced at the bottom face after 30 min and it can be seen that unlike the products at the top surface, the tops of these nanowires are sharp and needlelike. Formation of the nanosheets at the bottom surface after 45 min is also confirmed by the TEM image shown in Figure 5c. The transparent nature of the sheets indicates their small thickness. Figure 5d shows the branched ZnO structure formed at the edges after 30 min. The TEM image also reveals the rough surface and indicates the initiation of lots of new branches from the existing ones. The crystal structures of the ZnO nanonails and nanowires were further investigated through HRTEM images. The HRTEM images of both types of nanoforms reveal the wurtzite structure of ZnO and it is observed that the growth direction for both types of nanostructures is the (002) direction, in good agreement with the observations from XRD. Figure 5e shows one representative HRTEM image of one such nanoform revealing the growth direction to be (002). The corresponding selected area diffraction pattern (SAED) shown in the inset of Figure 5e also confirms the growth direction to be (002). Figure 5f shows the HRTEM image of a nanosheet along with the fast Fourier transformation (FFT) of the image in the inset. The measured spacing of the lattice fringes is 0.52 nm, corresponding to the (001) lattice plane of wurtzite ZnO. The HRTEM image of these nanoforms reveals a stacking fault-free single crystalline structure.

The growth of the ZnO nanoforms was based on the thermal evaporation condensation method. The growth of the 1-D nanoforms is generally governed by the catalytic VLS[22] or noncatalytic vapor−solid[23] approach. The role of the VLS method for the growth of ZnO 1-D nanoforms in our case could be ruled out as no catalyst was used. Instead the nucleation of the ZnO nanoforms could be attributed to a self-catalyzed VLS technique and the subsequent longitudinal growth was attributed to the vapor−solid growth. The complete growth process is nothing but a classical crystal growth mechanism. As the Zn species have taken an active part in the formation of ZnO 1-D nanoforms they could not be termed as catalyst in the true sense but in analogy with the catalytic action the term "self-catalyzed" has been used here. As the temperature was above the melting point of Zn (419 °C), the Zn powder evaporated and condensed on the substrate as a molten liquid droplet. This liquid Zn droplet served as the catalyst particle, which was the favorable site for the absorption of new Zn species and O_2. Continuous intake of the Zn and O_2 resulted in the formation of ZnO solid 1-D nanoforms. The role of the Zn droplets in the nucleation of the 1-D ZnO nanoforms was confirmed by the fact that when oxygen was introduced in the deposition system from the very beginning of the experiment no products were obtained. The formation of the ZnO nails indicated that the vapor−solid process might have played its part too. Initially ZnO nanorods were formed from the Zn droplets. The hexagonal cross-section, i.e., six defined facets, arose to maintain the minimum surface

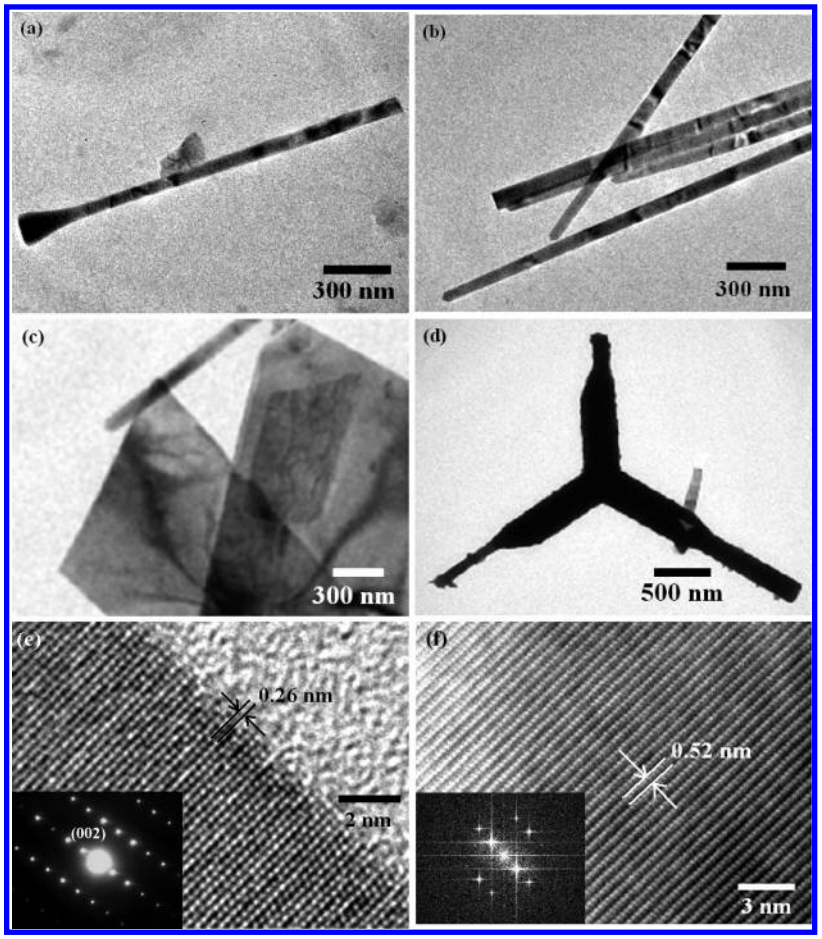

Figure 5. TEM images of the different nanoforms: (a) nanonails produced at the top surface after 30 min, (b) nanowires produced at the bottom surface after 30 min, (c) ZnO nanosheets produced along with the nanowires after 45 min, and (d) Branched ZnO nanoforms produced at the edge of the substrate after 30 min. HRTEM image of a single nanowire along with the corresponding SAED pattern is shown in part e. The image in part f shows the HRTEM pattern of the ZnO nanosheet with the corresponding FFT pattern in the inset.

energy and the crystal symmetry of the wurtzite ZnO. But, the presence of oxygen in the deposition system might have oxidized the Zn vapor to ZnO, which was deposited on the ZnO nanorods. The top cap area of the ZnO rods absorbed these ZnO vapor species, as it was the energetically favored area. Due to the high mobility at higher temperature the ZnO molecular species deposited to the base and surface area moved to the top area. In this way the top area grew not only in the longitudinal direction but also in the transverse direction resulting in the inflation of the cap area of the ZnO nanorods giving them a nail-like shape. The decrease of the diameters of the nanonails after 45 min of deposition might be due to insufficient vapor species. In the bottom face, due to the higher vapor pressure of Zn the growth initiated by the self-catalyzed VLS approach was very fast and as a result the ZnO species did not have sufficient time to be incorporated into the growth site. This was also evident from the fact that the length of the ZnO nanowires deposited after 30 min time was almost double those of the ZnO nanonails. As the nanowires became longer a longer bending contour appeared, which served as the energetically favorable site for the deposition of ZnO species resulting in the formation of ZnO nanosheets. Also the bending of the nanowires might have caused some interpenetrative growth between the nanowire tips or it might have formed some interconnected networks as was reported by Wang's group.[24,25] These interconnected regions acted as the favored site for the secondary two-dimensional growth giving rise to the foggy materials which grew with time to form nanosheets. At the edge the initially grown ZnO nanorod meets the Zn and ZnO vapor species from both the lateral and longitudinal direction. As a result both kinds of growth, viz., self-catalyzed VLS and VS, respectively, were quite strong and the surface of the nanoforms obtained was quite rough. These rough surfaces were much favored sites for the absorption of new vapor species resulting in the growth of ZnO nanotrees.

Figure 6a shows the room temperature optical absorbance spectrum of the ZnO nanowires recorded by dispersing the ZnO nanoforms in spectroscopic grade ethanol. All the samples showed almost similar nature in the optical absorption spectra. A sharp transition at 373 nm corresponding to 3.324 eV was observed in the optical absorbance spectrum. This corresponds to the bulk value of the band gap of ZnO. The absorption study revealed that the nanoforms were transparent in the visible region. Figure 6b shows the room temperature PL spectra of the ZnO nanonail and nanowire arrays with a 300 nm excitation wavelength. The PL spectrum shows a very weak UV and a strong, broad green emission peak at 3.25 and 2.49 eV, respectively. The zoomed view of the UV emission is shown in the inset of Figure 6b. The UV emission originated from the excitonic recombination corresponding to the band edge emission of ZnO. The origin of green luminescence from the undoped ZnO is associated with the intrinsic defect centers such as oxygen vacancy (V_O), zinc vacancy (V_{Zn}), zinc interstitial (Zn_i), oxygen interstitial (O_i), or antisite oxygen (O_{Zn}). Though the origin of the green emission is generally referred to the deep level or trapped state emission, there is no universally accepted mechanism. There are few hypotheses to explain the origin of the green emission. The commonly cited reason is that the green

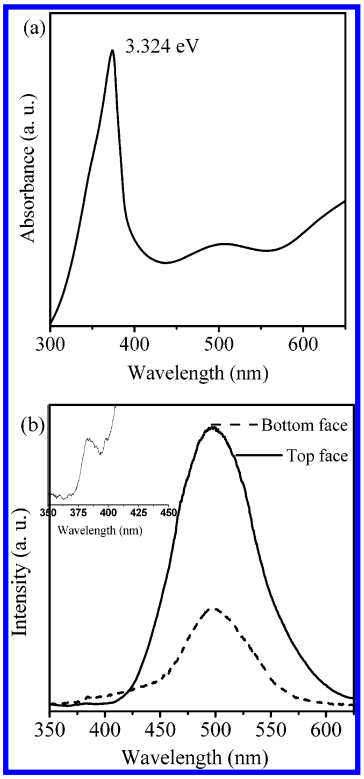

Figure 6. (a) Room temperature optical absorption spectrum of the ZnO nanowires. (b) Room temperature PL spectra of the ZnO nanonails and nanowire arrays.

emission originates due to the radiative recombination of a photogenerated hole with an electron occupying the oxygen vacancy.[26−28] Dijken et al.[29] reported that the green luminescence might be due to the transition from the conduction band to the deeply trapped hole. The donor−acceptor transitions are also reported[30,31] to be the origin of green emission. Complex defects involving transition from the zinc interstitial to the deep acceptor level like oxygen vacancy is another reason reported behind the green emission.[32] Lin et al.[33] have reported that oxygen antisite (O_{Zn}) could also induce green emission from ZnO.

It was observed that the emission from the top surface was much stronger than that of the bottom surface. Despite the fact that our sample has been prepared in an oxygen rich atmosphere, EDAX revealed oxygen deficiency in the samples. So, we believe that the transition from the conduction to the deep-level acceptor state is the reason behind the green emission from our samples. These PL spectra and the EDAX results also support our view about the self-catalyzed action of the Zn to form ZnO nanowire/nanonail arrays. When the synthesis was stopped suddenly the top portion of the 1-D ZnO nanoforms remained Zn rich and as a result the possibility of the generation of deep level defect centers such as oxygen vacancy and Zn interstitials increased.

In Figure 7 is shown the variation of log resistance as a function of inverse temperature for the sample characterized by the microstructure of Figure 2b. This is typical of all the samples studied. It is evident that the resistance variation reflects an activated process with the activation energy showing a variation with temperature. There are insufficient data, however, to be able to extract reliable terminal values of the activation energy.

Figure 8a shows the typical resistance change of a sample as a function of time when it was subjected to a gas mixture with N_2 of 200 ppm of CO at a temperature of 225 °C. It can be

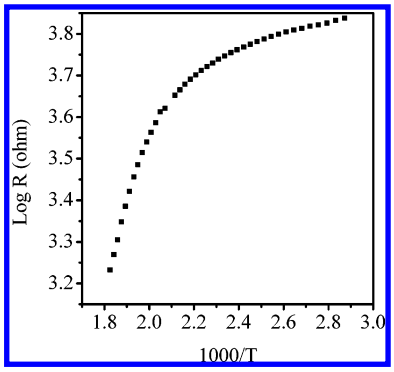

Figure 7. Log resistance versus inverse temperature plot for the ZnO nanonail array.

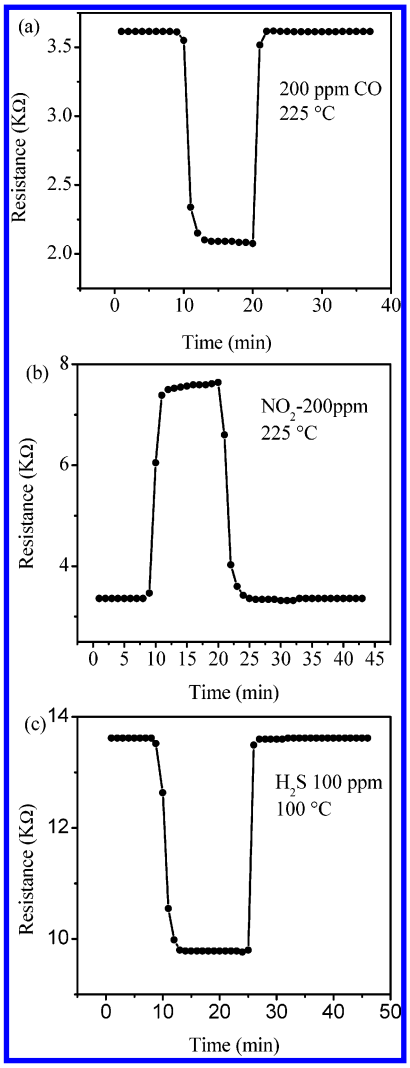

Figure 8. Change of dc resistance of the ZnO nanonail array as a function of time in different gases at different concentrations and temperatures: (a) 200 ppm of CO at 225 °C, (b) 200 ppm of NO_2 at 225 °C, and (c) 100 ppm of H_2S at 100 °C.

seen that the resistance decreases by a factor of ∼1.7. This arises because of the following reaction[34]

$$2CO + O_2^- \rightarrow 2CO_2 + e^- \quad (1)$$

which injects electrons into the conduction band. As a result the electron conductivity increases.

Figure 8b gives the resistance change with respect to time when sample was kept in an stream of 200 ppm of NO_2 in N_2

at a temperature of 225 °C. It is evident that there is an increase of resistance by a factor of 2. This can be explained on the basis of the following reaction

$$NO_2 + Zn \rightarrow ZnO + NO \quad (2)$$

The interstitial Zn atoms are oxidized to ZnO. This reduces the donor atoms, which in turn decreases the number of conduction electrons. Thus the electrical resistivity increases drastically.

In Figure 8c is shown the resistance change of the sample exposed to a gas stream containing 100 ppm of H_2S in N_2 at a temperature of 100 °C. It is seen that there is a decrease of sample resistance by a factor of ~1.4. This happens because of the reducing action of the H_2S, which injects electrons in the conduction band. The reaction concerned can be visualized as follows,

$$H_2S + O_2^- \rightarrow H_2 + SO_2 + e^- \quad (3)$$

It should be noted, however, that the sensing response is nonspecific. More data have to be collected as a function of the concentration of the different gaseous species before a firm conclusion regarding the gas sensing applications of these materials can be drawn.

4. Conclusions

In summary, ZnO nanowire and nanonail arrays have been synthesized by oxygen assisted thermal evaporation of metallic zinc on a quartz substrate over a large area. A self-catalyzed vapor−liquid−solid (VLS) process was believed to be operative here. The photoluminescence spectrum showed a weak UV and a broad green emission peak at 3.25 and 2.49 eV, respectively. The latter was attributed to the presence of zinc interstitial defects. Electrical resistance as a function of temperature indicated the activated mechanism to be operative. The samples showed reasonable sensing behavior with respect to CO, NO_2, and H_2S, respectively. CO and H_2S induced a lowering of electrical resistance whereas NO_2 increased the same.

Acknowledgment. One of the authors (B.N.P.) acknowledges an award of a Senior Research Fellowship by CSIR, New Delhi and D.C. thanks INSA, New Delhi for the award of a Scientist position. The research was supported by DST, New Delhi under the Nano Science and Technology Initiative.

References and Notes

(1) Banerjee, D.; Jo, S. H.; Ren, Z. F. *Adv. Mater.* **2004**, *16*, 2028.
(2) Li, S. Y.; Lin, P.; Lee, C. Y.; Tseng, T. Y. *J Appl. Phys.* **2004**, *95*, 3711.
(3) Sberveglieri, G.; Groppelli, S.; Nelli, P.; Tintinelli, A.; Giunta, G. *Sens. Actuators, B* **1995**, *25*, 588.
(4) Xiangfeng, C.; Dongli, J.; Djurisic, A. B.; Leung, Y. H. *Chem. Phys. Lett.* **2005**, *401*, 426.
(5) Rodriguez, J. A.; Jirsak, T.; Dvorak, J.; Sambasivan, S.; Fischer, D. *J. Phys. Chem. B* **2000**, *104*, 319.
(6) Ohta, H.; Kawamura, K.; Orita, M.; Hirano, M.; Sarukura, N.; Hosono, H. *Appl. Phys. Lett.* **2000**, *77*, 475.
(7) Aoki, T.; Hatanaka, Y.; Look, D. C. *Appl. Phys. Lett.* **2000**, *76*, 3257.
(8) Yokogawa, T.; Kamiyama, S.; Yoshii, S.; Ohkawa, K.; Tsujimura, A.; Sasai Y. *Jpn. J. Appl. Phys. Part 2* **1996**, *35*, L314.
(9) Huang, M. H.; Mao, S.; Feick, H.; Yan, H.; Wu, Y.; Kind, H.; Weber, E.; Russo, R.; Yang, P. *Science* **2001**, *292*, 1897.
(10) Ng, H. T.; Han, J.; Yamada, T.; Nguyen, P.; Chen, Y. P.; Meyyappan, M. *Nano Lett.* **2004**, *4*, 1247.
(11) Bai, X. D.; Gao, P. X.; Wang, Z. L.; Wang, E. G. *Appl. Phys. Lett.* **2003**, *82*, 4806.
(12) Wang, X.; Summers, C. J.; Wang, Z. L. *Nano Lett.* **2003**, *3*, 1315.
(13) Wang, X.; Song, J.; Li, P.; Ryou, J. H.; Dupuis, R. D.; Summers, C. J.; Wang, Z. L. *J. Am. Chem. Soc.* **2005**, *127*, 7920.
(14) Gao, P. X.; Ding, Y.; Wang, Z. L. *Nano. Lett.* **2003**, *3*, 1315.
(15) Lee, C. J.; Lee, T. J.; Lyu, S. C.; Zhang, Y.; Ruh, H.; Lee, H. J. *Appl. Phys. Lett.* **2002**, *81*, 3648.
(16) Lyu, S. C.; Zhang, Y.; Lee, C. J.; Ruh, H.; Lee, H. J. *Chem. Mater.* **2003**, *15*, 3294.
(17) Kim, T. W.; Kawazoe, T.; Yamazaki, S.; Ohtsu, M.; Sekiguchi, T. *Appl. Phys. Lett.* **2004**, *84*, 3358.
(18) Yao, B. D.; Chan, Y. F.; Wang, N. *Appl. Phys. Lett.* **2002**, *81*, 757.
(19) Wang, L.; Zhang, X.; Zhao, S.; Zhou, G.; Zhou, Y.; Qi, J. *Appl. Phys. Lett.* **2005**, *86*, 024108.
(20) Lao, J. Y.; Huang, J. Y.; Wang, D. Z.; Ren, Z. F. *Nano. Lett.* **2003**, *3*, 235.
(21) Guha, P.; Kar, S.; Chaudhuri, S. *Appl. Phys. Lett.* **2004**, *85*, 3851.
(22) Wagner, R. S.; Ellis, W. C. *Appl. Phys. Lett.* **1964**, *4*, 89.
(23) Sears, G. W. *Acta Metal* **1955**, *3*, 361.
(24) Yang, R.; Wang, Z. L. *Solid State Commun.* **2005**, *134*, 741.
(25) Gao, P. X.; Lao, C. S.; Hughes, W. L.; Wang, Z. L. *Chem. Phys. Lett.* **2005**, *408*, 174.
(26) Dai, Y.; Zhang, Y.; Li, Q. K.; Nan, C. W. *Chem. Phys. Lett.* **2002**, *358*, 83.
(27) Vanheusden, K.; Warren, W. L.; Seager, C. H.; Tallant, D. R.; Voigt, J. A.; Gnade, B. E. *J. Appl. Phys.* **1996**, *79*, 7983.
(28) Huang, M. H.; Wu, Y.; Feick, H.; Tran, N.; Weber, E.; Yang, P. *Adv. Mater.* **2001**, *13*, 113.
(29) van Dijken, A.; Meulenkamp, E.; Vanmaekelbergh, D.; Meijerink, A. *J. Phys. Chem. B* **2000**, *104*, 1715.
(30) Studenikin, S. A.; Cocivera, M. *J. Appl. Phys.* **2002**, *91*, 5060.
(31) Reynolds, D. C.; Look, D. C.; Jogai, B. *J. Appl. Phys.* **2001**, *89*, 6189.
(32) Korsunska, N. O.; Borkovska, L. V.; Bulakh, B. M.; Khomenkova L. Y.; Kushnirenko, V. I.; Markevich, I. V. *J. Lumin.* **2003**, *102*, 733.
(33) Lin, B.; Fu, Z.; Jia, Y. *Appl. Phys. Lett.* **2001**, *79*, 943.
(34) Baraton, M. I.; Merhari, L. *Rev. Adv. Mater. Sci.* **2003**, *4*, 15.